The Differential Capacitance of Ionic Liquid | Metal Electrode Interfaces – A Critical Comparison of Experimental Results with Theoretical Predictions

Jens Wallauer, Marcel Drüschler, Benedikt Huber, and Bernhard Roling

Department of Chemistry, Philipps University of Marburg, Hans-Meerwein-Strasse, 35032 Marburg, Germany

Reprint requests to Prof. Dr. Bernhard Roling. Fax: +49 6421 282 2309.
E-mail: roling@staff.uni-marburg.de

Z. Naturforsch. **2013**, *68b*, 1143 – 1153 / DOI: 10.5560/ZNB.2013-3153
Received June 13, 2013

Results of potential-dependent differential capacitance measurements on the interface between six different ionic liquids and the (111) surface of single-crystalline gold are presented. The measurements were done by means of broadband impedance spectroscopy in a frequency range from 10 mHz to 1 MHz. We discuss the influence of the IL cation, the IL anion and the cations' alkyl chain length on the interfacial capacitance. Our results suggest that (i) there is no simple relationship between the cation size and the value of the differential capacitance, (ii) the general shape of the potential-dependent differential capacitance curve is more strongly influenced by the IL anion, and (iii) experimental differential capacitance curves do not exhibit a simple "camel-" or "bell-shaped" curvature as predicted by mean-field theories. Furthermore, the broadband measurements show that two capacitive processes can be distinguished, which take place on millisecond and second time scales, respectively. While a millisecond time scale is expected for double-layer charging governed by the bulk conductivity of the IL, the existence of a slow process points to additional barriers for charge transport at the interface. The capacitance contribution of the slow process is most pronounced for ILs based on the *N*-butyl-*N*-methyl-pyrrolidinium ([$Pyr_{1,4}$]) cation. A comparison of capacitance data with *in-situ* STM data from previous studies suggests that the slow process is connected to herringbone-type structures at the interface. While the herringbone superstructure of the Au(111) surface is well known in aqueous electrochemistry, a herringbone-type structure of adsorbed ions was described in a recent MD simulation paper by Federov and coworkers (K. Kirchner, T. Kirchner, V. Ivaništšev, M. V. Fedorov, *Electrochim. Acta* **2013**, in press: doi: 10.1016/j.electacta.2013.05.049).

Key words: Ionic Liquid, Au(111), Interface, Differential Capacitance, Electrochemical Impedance Spectroscopy

Introduction

Many ionic liquids show good ionic conductivities, moderate viscosities and broad electrochemical stability windows up to 6 V [1 – 3]. Moreover, ionic liquids are typically non-flammable and thermally stable up to high temperatures [2]. By changing the functional groups of cations and by varying the cation/anion combination, these physico-chemical properties can be adjusted to particular requirements. Thus, ionic liquids have often been called *designer solvents*. In electrochemistry, ionic liquids are seen as promising electrolytes for manifold applications, *e. g.* for electrosynthesis [4, 5], for electro-analysis [4, 6], for electrodeposition of metals [7 – 9], for energy storage in batteries and supercapacitors [10 – 13], for energy conversion in dye sensitized solar cells [14], and for double-layer field-effect transistors [15]. A common and central aspect of all applications is the important role of the structure and dynamics of the interface between ionic liquids and the chosen electrode materials; see for instance ref. [16].

Since ILs are highly concentrated ionic fluids, the interface cannot be described theoretically by the classical Stern model for diluted electrolytes, in which the ions are treated as point charges. In 2007, A. A. Kornyshev presented an elegant way to take into account the finite volume of the ions in dense systems [17]. In

his mean-field lattice-gas model, the ions are placed onto the sites of a cubic lattice in front of a charged surface. By admitting free sites (voids), the ion density can be adjusted. Thus, a central parameter of the model is the site occupation number γ, which is defined as the ratio of occupied sites to all sites. Coulomb interactions of the ions with the charge surface and with other ions are taken into account only at the mean field level, while other types of interactions, such as dispersion interactions and hydrogen bonding, are neglected. Consequently, the expression for the free energy of the system consists of only two contributions: (i) the electrostatic work for moving ions in a mean-field electrical potential and (ii) the entropy for arranging the ions on the available sites. From this expression, the differential capacitance of the IL | electrode interface can be calculated, which is defined as the derivative of the electrode's charge q with respect to the electrode potential E at constant pressure p, temperature T and chemical potentials of the ions μ_i (Eq. 1).

$$C = \left.\frac{\partial q}{\partial E}\right|_{p,T,\mu_i} \tag{1}$$

In this mean-field model, the differential capacitance C is determined by the entropy penalty for accumulating charge at the interface. Depending on the site occupation number γ, potential-dependent differential capacitance curves exhibit either a camel-type shape or a bell-type shape; see Fig. 1. At rather low site occupation numbers, such as $\gamma = 0.1$, the entropy penalty for charge accumulation first decreases with increasing $|E|$ around $E = 0$ (pzc = potential of zero charge in this model), and then increases with increasing charge density at the interface. When the site occupation number is close to unity (blue curve), there is an increasing entropy penalty for successive charge accumulation at the interface leading to the bell-type shape. Consequently, for ionic liquids with high ion densities, the mean-field lattice gas model predicts a bell-type shape. When taking typical values for the bulk concentration of ions in ILs, here: 3.9 mol L^{-1}, and for the permittivity in the double-layer, here: $\varepsilon_r = 4$, very large values for the differential capacitance in the range of 150 – 250 μF cm^{-2} are obtained around the pzc. These values are much higher than typical values obtained in experiments (5 – 15 μF cm^{-2}). The reason for this discrepancy is primarily the neglect of the potential drop between the electrode surface and the center of charge of the ions in the innermost layer. This

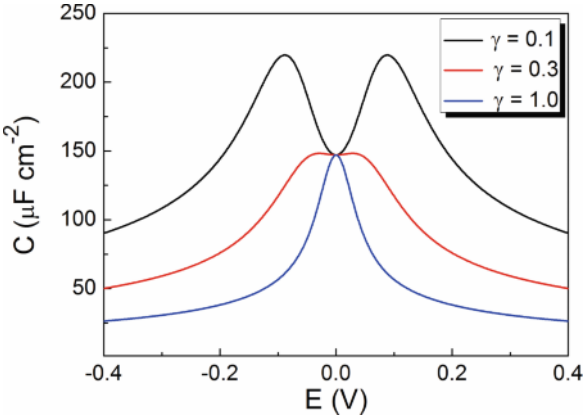

Fig. 1 (color online). Differential capacitance curves $C(E)$ predicted by Kornyshev's mean-field lattice gas model for site occupation numbers $\gamma = 0.1$, 0.3 and 1. $c(\infty)$ was set to 3.9 mol L^{-1}, which is a typical value for ionic liquids, and ε_r was assumed to have a value of 4 at the interface [17], which is smaller than typical bulk values [22] due to a strong electric field close to the electrode surface [23].

potential drop can be taken into account by means of a Helmholtz capacitance in series to the capacitance shown in Fig. 1. This leads to much lower differential capacitance values and to a much weaker potential dependence [18].

In subsequent publications, some modifications of the original model were considered, and alternative models were published. Fawcett and Ryan took into account the compressibility of the diffuse part of the interface as well as the local variation of the electric field [19]. Bazant, Storey and Kornyshev accounted for short-range Coulomb interactions between the ions [20]. Shklovskii and coworkers emphasize the importance of interactions between individual ions and their image charge in the metal surface and thus go beyond the mean-field approximation [21].

The published experimental capacitance data are quite diverse and in some cases even contradictory [24]. Possible reasons have been discussed in detail by Lockett and coworkers [24], who considered the ionic liquid purification procedure, the reference electrode stability, the surface of electrode materials, and the methods for extracting capacitance data from EIS results. Thus, it is important to carry out studies on the interface between well-defined electrodes and very pure ionic liquids and to establish suitable methods for the extraction of capacitance data from broadband EIS spectra.

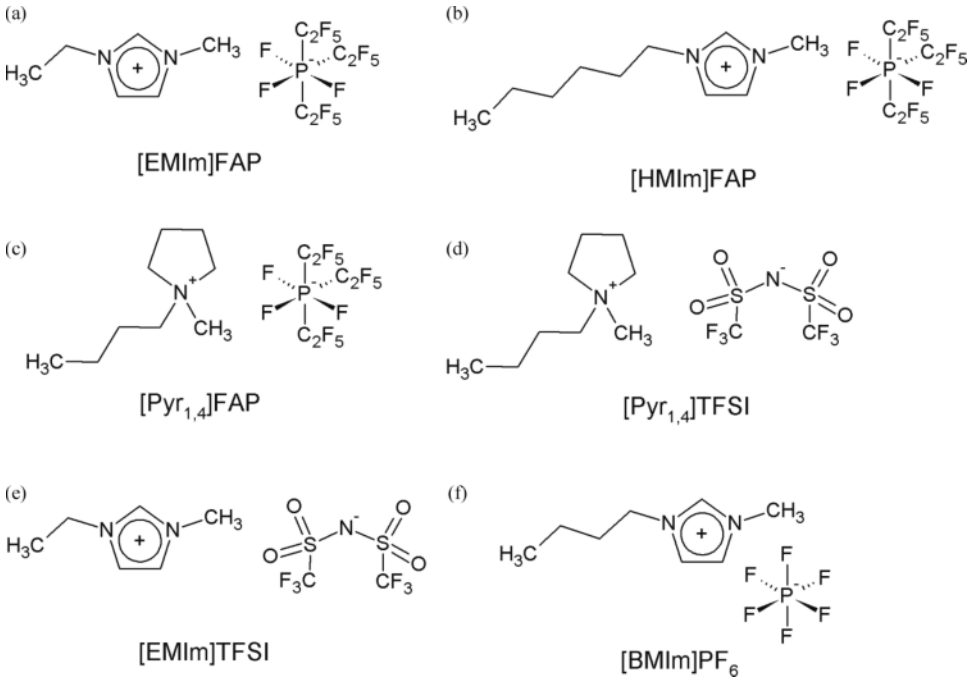

Fig. 2. Chemical structure of the six ionic liquids used in this study.

In this paper, we present the results of electrochemical studies on the interface between the (111) surface of single-crystalline Au and six different ionic liquids using cyclic voltammetry and broadband EIS. The chemical structure of the cations and anions in the following six ILs are sketched in Fig. 2: 1-ethyl-3-methyl-imidazolium tris(pentafluoroethyl)trifluorophosphate [EMIm]FAP, 1-hexyl-3-methyl-imidazolium tris(pentafluoroethyl)trifluorophosphate [HMIm]FAP, *N*-butyl-*N*-methyl-pyrrolidinium tris(pentafluoroethyl)-trifluorophosphate [$Pyr_{1,4}$]FAP, *N*-butyl-*N*-methyl-pyrrolidinium bis(trifluoromethanesulfonyl)imide [$Pyr_{1,4}$]TFSI, 1-ethyl-3-methyl-imidazolium bis(trifluoromethanesulfonyl)imide [EMIm]TFSI, and *N*-butyl-*N*-methyl-imidazolium hexafluorophosphate [BMIm]PF_6. These ionic liquids have been chosen for several reasons: (i) Imidazolium- and pyrrolidinium-based ILs are promising candidates for the use as electrolytes in many electrochemical applications, since these cations are quite stable towards reduction and oxidation, (ii) the same applies to the FAP^-, $TFSI^-$, and PF_6^- anions, (iii) the FAP-based ILs with three different cations allow for studying the influence of the cation on the interfacial properties, (iv) the investigation of two ILs composed of the *N*-butyl-*N*-methyl-pyrrolidinium cation and different anions provides an insight into the influence of the anion, and (v) the comparison of data obtained for [EMIm]FAP, [BMIm]PF_6 and [HMIm]FAP provides information about the influence of the cations' alkyl chain length.

Potential-dependent differential capacitance data were extracted from broadband impedance spectra in the following way [25, 26]: (i) conversion of complex impedance data into complex capacitance data; (ii) fit of the complex capacitance data with an empirical Cole-Cole equation. The obtained capacitance curves are critically compared with theoretical predictions of mean-field models [17, 19, 20]. Moreover, general trends regarding the influence of the IL anion and cation on the capacitance curves are highlighted.

Results and Discussion

In Fig. 3, cyclic voltammograms (CVs) of the different IL | Au(111) interfaces are depicted. The CVs on the top (marked with letters a–f) show extended scans for the determination of the electrochemical window, while those immediately below show the potential win-

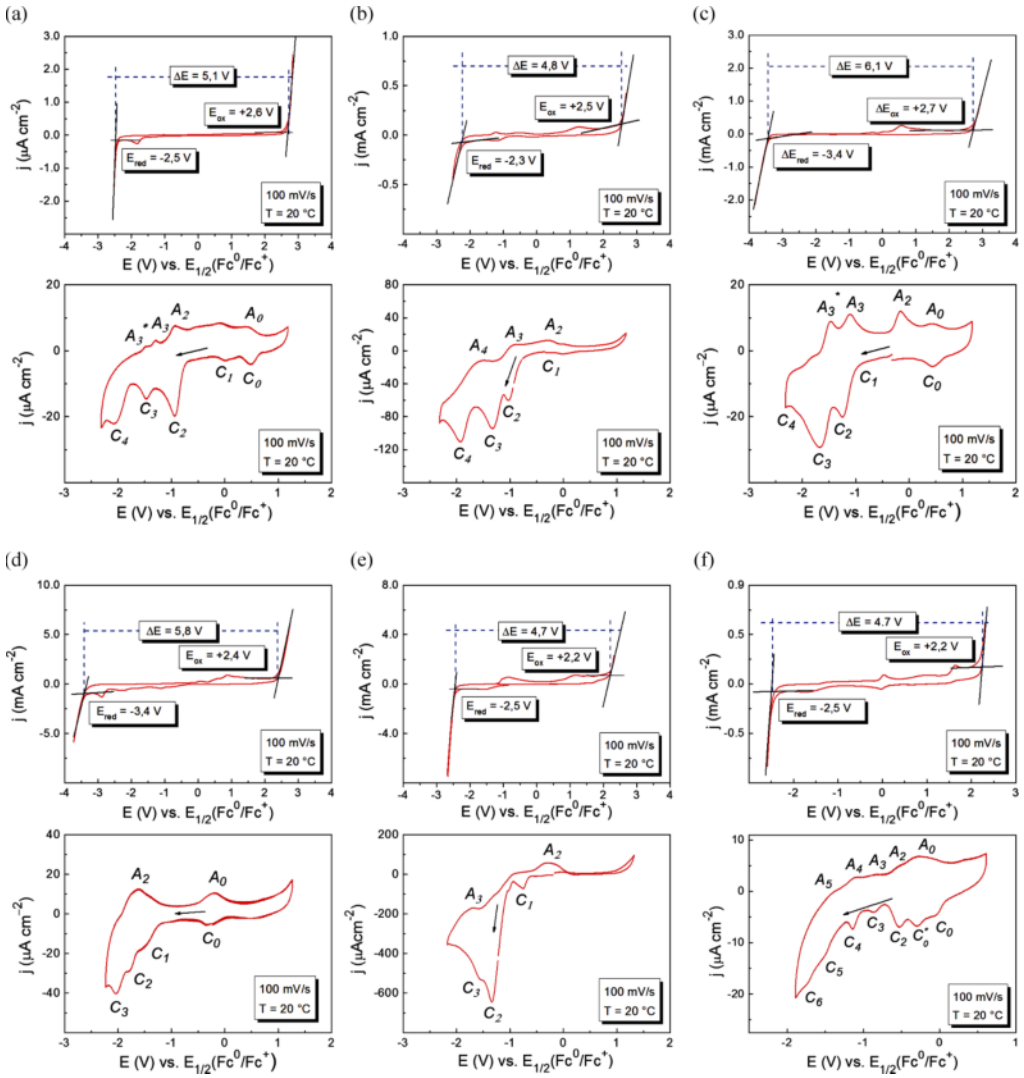

Fig. 3 (color online). Cyclic voltammograms (CVs) of the systems (a) [EMIm]FAP | Au(111), (b) [HMIm]FAP | Au(111), (c) [$Pyr_{1,4}$]FAP | Au(111), (d) [$Pyr_{1,4}$]TFSI | Au(111), (e) [EMIm]TFSI | Au(111), and (f) [BMIm]PF_6. The CVs depicted on the top (and marked with letters a–f) illustrate the electrochemical stability windows, while those immediately below show a zoom into the potential range which has been chosen for the EIS measurements. All data were recorded with a scan rate of 100 mV s^{-1} at a sample temperature of 20 °C.

dow in which the subsequent EIS measurements were performed.

In contrast to the commonly applied definition of the electrochemical window by choosing current density limits typically in the range of 1 – 5 mA cm^{-2} [27], we have used an alternative method based on a geometric construction: By drawing tangents to both sides of the cyclic voltammogram right before the steep increase of the current density occurs, and by additionally drawing tangents into the increasing parts, intersection points were determined, see left side of Fig. 3. The respective values for cathodic and anodic stability limits as well as for the overall electrochemical window are listed in Table 1.

The following trends are found: (i) all imidazolium-based ILs exhibit similar cathodic stability limits; (ii) all pyrrolidinium-based ILs exhibit similar cathodic stability limits; (iii) the pyrrolidinium-based ILs are

Table 1. Cathodic and anodic stability limits as well as overall electrochemical windows for the six ILs used in this study. The potentials are given with respect to the half wave potential of the ferrocene/ferrocinium redox couple. Literature values are added for comparison.

IL	E_{red} *vs.* $E_{1/2}$ (Fc^0/Fc^+) (V)	E_{ox} *vs.* $E_{1/2}$ (Fc^0/Fc^+) (V)	ΔE (V)
[EMIm]FAP	−2.5	+2.6	5.1
[HMIm]FAP	−2.3 (−2.6 [27])	+2.5 (+2.0 [27])	4.8
[$Pyr_{1,4}$]FAP	−3.4	+2.7	6.1
[$Pyr_{1,4}$]TFSI	−3.4 (−2.8 [27])	+2.4 (+1.4 [27])	5.8
[EMIm]TFSI	−2.5 (−2.2 [27])	+2.2 (+2.0 [27])	4.7
[BMIm]PF_6	−2.5 (−2.7 [27])	+2.2 (+2.1 [27])	4.7

more stable against reduction than the imidazolium-based ILs; (iv) the stability against oxidation depends mainly on the nature of the anion and increases in the order $FAP^- > TFSI^- \approx {PF_6}^-$. While these trends have also been found in other studies, the exact values of the anodic and cathodic stability limit differ for different studies [27–29]. This is most likely due to the usage of different electrode materials and due to different definitions of the electrochemical window.

In Fig. 3, the CVs immediately below the extended CVs show magnifications of the potential range, where mainly capacitive currents due to double-layer charging and small current density peaks are observed. We note that the peak position and peak current densities are quite characteristic for the different ILs and can thus be seen as a fingerprint of the respective IL | Au(111) interface. The peaks observed in cathodic scan direction are denoted as C_n, while those observed in anodic direction are denoted as A_n. The same index n indicates that the respective cathodic and anodic current density peaks are based on the same redox process. A discussion of the origin of these current density peaks is beyond the scope of the present paper. For the systems [EMIm]FAP | Au(111) and [$Pyr_{1,4}$]FAP, possible explanations can be found in references [25, 26, 30].

For the EIS measurements, the following procedure was applied: (i) in a first experiment starting from the open circuit potential, the potential was changed in cathodic direction in steps of 10 mV. At any dc potential, an impedance spectrum was taken by superimposing an ac voltage of 10 mV (rms) and varying the frequency from 1 MHz to 0.01 Hz. (ii) After preparing a fresh IL | Au(111) interface, this was repeated for a change of the potential in anodic direction. (iii) The individual complex impedance spectra were converted to complex capacitance spectra and plotted in the complex capacitance plane (CCP). In Fig. 4a, we show exemplarily a CCP spectrum of the [Pyr_{14}]FAP | Au(111) interface at a dc potential of −0.96 V *vs.* Fc^0/Fc^+. Clearly, two semicircles reflecting two ca-

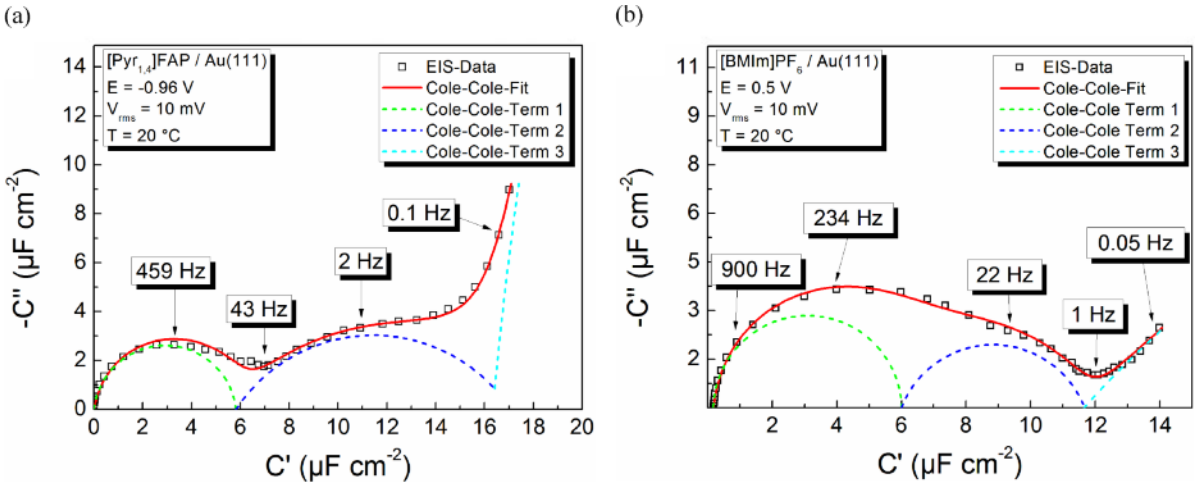

Fig. 4 (color online). Complex capacitance plane of two different systems: a) [Pyr_{14}]FAP | Au(111) at an electrode potential of −0.96 *vs.* $E_{1/2}(Fc^0/Fc^+)$. Here, a fast and a slow capacitive process can be clearly distinguished, while at low frequencies the onset of an ultraslow process is detected. b) [BMIm]PF_6 | Au(111) at a potential of +0.5 V *vs.* $E_{1/2}$ (Fc^0/Fc^+). Here, the extensive overlap between the fast and slow capacitive semicircle leads to uncertainties regarding the capacitance contribution of these processes.

pacitive processes taking place on different time scales can be distinguished. Furthermore, below 1 Hz, the high-frequency part of an ultraslow process is detected. In order to determine the capacitance contribution of the two capacitive processes, ΔC_{fast} and ΔC_{slow}, and their relaxation times, τ_{fast} and τ_{slow}, the spectra were fitted with an empirical Cole-Cole equation, as explained in detail in the Experimental Section. We note that the existence of more than one capacitive process at electrolyte | metal interfaces has also been reported by Pajkossy and co-workers [31–33].

Fig. 5 illustrates the potential dependence of ΔC_{fast} and ΔC_{slow} for the different IL | Au(111) interfaces. While the fast process taking place on millisecond time scales is found for all ILs over the entire potential range, the slow process with a time scale in the range of seconds is mainly observed for the pyrrolidinium-based ILs in the cathodic regime. We note that often the standard error of the fitting parameter ΔC_{slow} is very large, since there is significant overlap between the complex capacitance of the different processes as shown in Fig. 4b. For instance, in the case of [EMIm]FAP, the complex capacitance spectra in the potential range from −1 V to 0 V give strong indications for the existence of a slow capacitive process, but the standard error of ΔC_{slow} is almost as large as ΔC_{slow} (Fig. 5).

Now we first consider trends in the potential dependence of ΔC_{fast}: (i) For all systems, the curves are more complex than the bell-shaped or camel-shaped curves obtained from mean field theories. (ii) Overall, there is a relatively weak dependence of ΔC_{fast} on the electrode potential with typical capacitance values being in the range from 6–10 μF cm^{-2}. This was also found in many molecular dynamics simulation studies and in DFT calculations [34–42]. (iii) However, there are very characteristic features in the capacitance curves of some ILs. The TFSI-based ILs show a significant drop of the capacitance in the cathodic range (in the range −1 V to −2 V *vs.* Fc^0/Fc^+). [BMIM]PF_6 shows a characteristic maximum in the anodic range (around +0.5 V *vs.* Fc^0/Fc^+). (iv) There is a remarkable trend in the differential capacitance of the imidazolium-based ILs. The differential capacitance in the cathodic range, where the cations are enriched at the interface, decreases in the order [HMIm]FAP > [BMIm]PF_6 > [EMIm]FAP. This is exactly the opposite order one would expect from the size of the cations [HMIm] > [BMIm] > [EMIm]. Thus, it is obvious that apart from the cation size other factors, likely the cation flexibility and polarizability, play an important role for the capacitance. (v) In the anodic regime, the size of the anions seems to play an important role. As expected from the sizes $FAP^- > TFSI^- > PF_6^-$, there is a clear trend that the capacitance decreases in the order $PF_6^- > TFSI^- > FAP^-$.

The capacitance contribution of the slower process taking place on time scales in the range of seconds is largest in the cathodic regime of pyrrolidinium-based ILs. Thus, the interactions of pyrrolidinium cations with the electrodes and possibly also cation-cation interactions appear to be important for this peak. The peak potential is clearly related to the potential range where in previous *in situ* STM studies herringbone-type structure on the Au(111) surface have been observed. In the case of [$Pyr_{1,4}$]FAP, we find a maximum of ΔC_{slow} around −1 V *vs.* Fc^0/Fc^+ (Fig. 5c). In this potential range, the Endres group observed a herringbone structure on the entire Au(111) surface [30]. In the case of [$Pyr_{1,4}$]TFSI, the ΔC_{slow} peak maximum (Fig. 5d) and the herringbone structure [43] are observed at more cathodic potentials around −1.7 V *vs.* Fc^0/Fc^+.

The herringbone reconstruction of Au surfaces is well known from aqueous electrochemistry [45]. When a flame-annealed reconstructed Au surface is immersed in an aqueous electrolyte, the surface remains reconstructed as long as there is no specific adsorption of anions. In the [$Pyr_{1,4}$]-based ILs, the situation is quite different. At the ocp, which is around −0.05 V *vs.* Fc^0/Fc^+, no herringbone reconstruction is detected by *in-situ* STM imaging. As already mentioned, the completely reconstructed surface can be imaged around −1 V and around −1.7 V, but seems to disappear again at higher cathodic potentials [30]. Thus the physical origin of the herringbone reconstruction in ILs is not clear at present.

In this context it is interesting to note that in a recent paper, Federov and coworkers [44] have suggested that the herringbone structure detected by *in situ* STM might be a structure formed by adsorbed cations. In a molecular dynamic simulation of an IL | electrode interface, they detect a transition from a multilayer ion structure to ordered single-layer or to ordered two-layer ion structures at particular values of the electrode charge density. When the electrode charge density is well below the charge density of a monolayer of adsorbed ions, overscreening effects are important

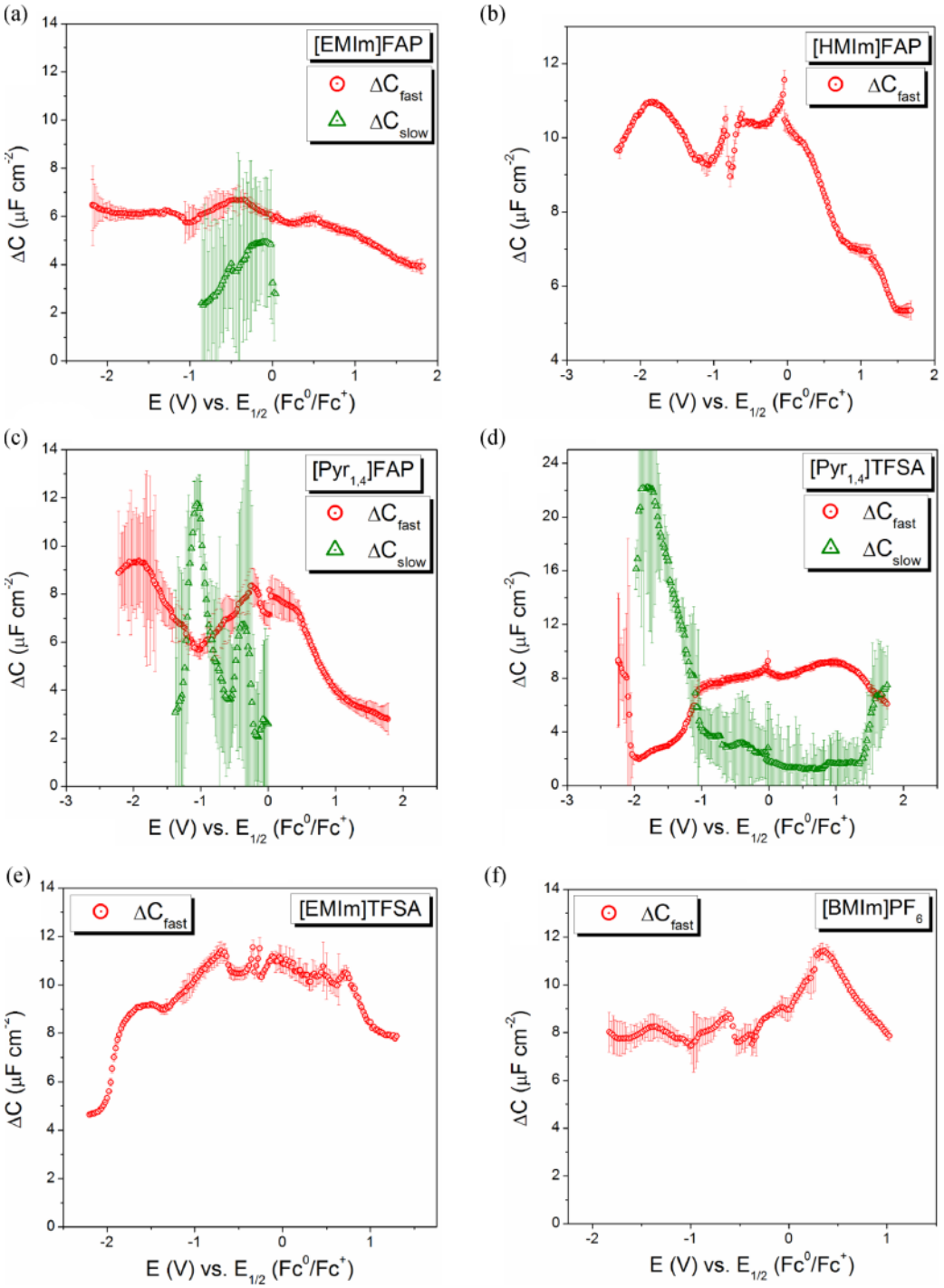

Fig. 5 (color online). Differential capacitance of the fast capacitive process ΔC_{fast} (red circles) and of the slow capacitive process ΔC_{slow} (green triangles) *vs.* the electrode potential, which is given with respect to the half wave potential of the ferrocene/ferrocenium redox couple. The capacitance of the slow capacitive process is only shown in potential ranges where this process is clearly visible in the spectra.

leading to multilayer structures with pronounced spatial charge density oscillations. However, when the electrode charge is close to an integer multiple of an ion monolayer charge, well-ordered single-layer (integer = 1) or two-layer structures (integer = 2) are observed. In a certain charge density range around the integer value of 2, the two-layer interface exhibits a herringbone-type structure.

Considering all these experimental and theoretical results, we suggest that the following important issues should be addressed in the future: (i) It should be clarified experimentally whether the herringbone structure at the Au(111) | IL interface is formed by Au atoms or by adsorbed cations. To this end, STM and AFM imaging of the interfacial structures with atomic resolution would be desirable, which is definitely not an easy task. (ii) The scientific community active in this field should try to agree on experimental protocols and analysis methods for obtaining reproducible and reliable results for the differential capacitance of metal | IL interfaces. Even with the same complex impedance data, different capacitance values are obtained, when single-frequency analyses, analyses based on CPE elements or, like in our case, Cole-Cole fitting of data in the complex capacitance plane are carried out. For instance, in the case of [BMIm]PF_6 we find that the capacitance in the anodic range is higher than in the cathodic range, while the opposite trend was reported in [24]. (iii) For a comparison of experimental data with theoretical models, experimental knowledge about the potential of zero charge (pzc) is important. In diluted electrolytes, the pzc can be easily determined from the minimum in the potential-dependent differential capacitance curves [46], however in the case of ILs, this method is not applicable. Thus, alternative methods, such as contact angle measurements [47 – 50] and immersion techniques [51, 52] have to be adapted to ILs, and new methods have to be developed.

Conclusions

We have measured frequency-dependent capacitance spectra of the interface between six ionic liquids and a well-defined Au(111) surface. The spectra reveal the existence of two capacitive processes taking place on millisecond and on second time scales, respectively. The contribution of the two processes to the interfacial capacitance, ΔC_{fast} and ΔC_{slow}, depends on the electrode potential.

The potential-dependent shape of ΔC_{fast} is primarily determined by the anions. As expected from the sizes FAP^- > $TFSI^-$ > $PF_6{}^-$, there is a clear trend that the capacitance in the anodic regime decreases in the order $PF_6{}^-$ > $TFSI^-$ > FAP^-. For the imidazolium-based ILs, the differential capacitance in the cathodic range decreases in the order [HMIm]FAP > [BMIm]PF_6 > [EMIm]FAP. This is remarkable, since the opposite trend would have been expected from the size of the cations [HMIm] > [BMIm] > [EMIm]. Overall, the potential dependence of ΔC_{fast} is relatively weak as described by DFT calculations and as seen in many MD simulations. In contrast, simple mean-field theories predict a much stronger potential dependence.

The capacitance contribution of the slow process ΔC_{slow} is strongest for the [$Pyr_{1,4}$]-based ILs in the cathodic range. For both ILs, a $\Delta C_{slow}(E)$ peak is detected exactly in the respective potential range, where *in-situ* STM studies reveal the existence of herringbone-type structures on the gold surface. While a herringbone reconstruction of gold surfaces in aqueous electrolytes is well known, there is little knowledge about surface reconstruction and lifting in ILs. A recent MD simulation by Federov and coworkers has indicates that herringbone-type structures may also be formed by adsorbed ions. Thus, more work in the high-resolution imaging of interfacial structures by means of *in-situ* STM and AFM techniques is needed in order to clarify the nature of the herringbone reconstruction in these ILs.

For a better comparison of experimental and theoretical results, an experimental determination of the potential of zero charge (pzc) would be highly desirable. To this end, methods known from aqueous electrochemistry, like contact angle measurements and immersion techniques, have to be adapted to ILs, and new methods have to be developed.

Experimental Section

Five ILs were purchased from Merck KGaA ([EMIm]FAP, [HMIm]FAP, [$Pyr_{1,4}$]FAP) and from Iolitec ([EMIm]TFSI, [BMIm]PF_6). [$Pyr_{1,4}$]TFSI was synthesised by Passerini *et al.* by means of a method described in [53, 54]. The FAP^- ILs were dried for several hours under vacuum (10^{-3} mbar) at 100 °C by the Endres group in Clausthal and sent to Marburg in sealed sample containers. The $TFSI^-$ and $PF_6{}^-$ ILs were dried in Marburg at a pressure of 10^{-6} mbar at elevated temperatures of 50 – 80 °C

for at least 24 h. All ILs were strictly handled and stored in inert gas atmosphere (N_2 or Ar) in a glove box (LABStar, MBraun GmbH). For all ILs, the remaining water content was less than 15 ppm as measured by Karl-Fischer titration (Mettler-Toledo, C20 Coulometric Karl-Fischer-Titrator). It should be noted that for coulometric Karl-Fischer titrations with small amounts of liquids, this is well inside the range of the detection limit which is typically around 20 – 25 ppm (or around 10 μg of water) [55].

The working electrode consisted of a thin ($\sim$ 200 nm) Au(111) layer on a mica substrate and was purchased either from Agilent Technologies or from Phasis. A round, polycrystalline platinum electrode (Goldschmiede Meusser, Marburg, Germany) was used as counter electrode. A custom-built micro-reference electrode based on Ag | AgTFSI | [EMIm]TFSI [56] served as a stable reference electrode. The electrode was inserted into the cell through a small hole in the counter electrode. When the EIS part of an experiment had been performed, the potential of the reference electrode was checked by measuring a cyclic voltammogram after adding a small amount of 10 mmol L^{-1} ferrocene solution in the IL under study.

All electrochemical measurements were recorded using a PotGAL 10V/15A potentiostat connected to an Alpha high-performance frequency analyzer (Novocontrol). The measurement cell consisted of a sample holder for the Microcell HC (rhd instruments) platform (Fig. 6). The working electrode was fixed on top of a gold-plated copper base by means of a spring which also served as an electric contact. An O-ring (Viton, Kremer GmbH) was clamped onto the working electrode by a polyether ether ketone (PEEK) cover. The O-ring prevents the leakage of the measurement cell and at the same time limits the active surface of the working electrode to 0.38 cm^2. The entire measurement cell had a volume of $\sim$ 50 μL. The Microcell HC platform allows a quick and accurate temperature control by heating or cooling the cell *via* a Peltier element and by measuring the temperature *via* a Pt100 probe inside the gold-plated copper base of the sample holder.

A measurement protocol consisted of two steps. After assembly of the cell and before carrying out the EIS measurements, a cyclic voltammogram within the respective ILs stability window was recorded with a scan rate of 100 mV s^{-1}. Starting from the open circuit potential, the DC potential was then swept in 10 mV or 20 mV steps either in anodic or cathodic direction. After every potential step, the system was given 10 min of equilibration time before the EIS measurement was started. An impedance spectrum with V_{rms} = 10 mV was recorded at every DC potential at frequencies ranging from 10^6 Hz to 0.01 Hz. Afterwards, a fresh Au(111) sample was used in the same manner for the other scan direction. The measured impedance spectra were transformed

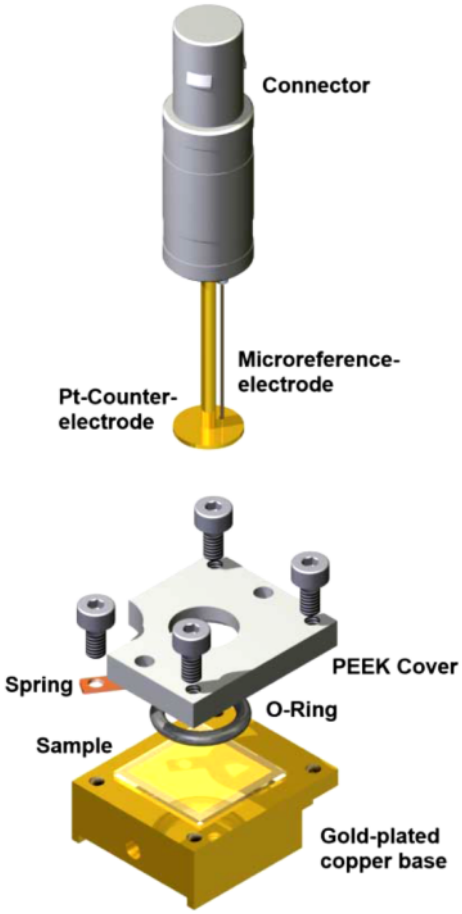

Fig. 6 (color online). Sample holder (rhd instruments) for the CV and EIS measurements, consisting of a gold-plated copper base, a PEEK cover and a connector for the Pt counter electrode and for the micro-reference electrode.

into the complex capacitance by means of Eq. 2 and analyzed by fitting the spectra to a sum of Cole-Cole expressions (Eq. 3).

$$\hat{C}(\omega) = \frac{1}{i\omega\hat{Z}(\omega)} \tag{2}$$

$$\left(\hat{C}(\omega) - C_\infty\right) = \sum_{i=1}^{n} \frac{\Delta C_i}{1 + (i\omega\tau_i)^{\alpha_i}} \tag{3}$$

Every Cole-Cole term represents a suppressed ($0 < \alpha_i < 1$) or ideal ($\alpha_i = 1$) semicircle in the complex capacitance plane. The Cole-Cole fit provides information about the capacitance contribution of the process i, ΔC_i, and about its time constant τ_i.

Acknowledgement

This work was financially supported by the Deutsche Forschungsgemeinschaft (DFG) within the Priority Program SPP 1191 "Ionic Liquids" and by the Fonds der Chemischen Industrie (PhD stipend for M. D.). We thank Frank Endres and Natalia Borisenko for providing the high-purity ionic liquids and for helpful discussions about the influence of impurities on IL | electrode interfaces. We thank Stefano Passerini for providing [$Py_{1,4}$]TFSI in high purity. Furthermore, we are grateful to Axel Braam (Sundermeyer group, Marburg) for performing Karl-Fischer titrations. Finally, we thank Maxim Federov for helpful discussions on the structure of adsorbed ions at IL | electrode interfaces.

[1] M. C. Buzzeo, R. G. Evans, R. G. Compton, *Chem. Phys. Chem.* **2004**, *5*, 1106 – 1120.
[2] F. Endres, S. Z. El Abedin, *Phys. Chem. Chem. Phys.* **2006**, *8*, 2101 – 2116.
[3] M. Galiski, A. Lewandowski, I. Stpniak, *Electrochim. Acta* **2006**, *51*, 5567 – 5580.
[4] M. C. Buzzeo, R. G. Evans, R. G. Compton, *Chem. Phys. Chem.* **2004**, *5*, 1106 – 1120.
[5] P. Hapiot, C. Lagrost, *Chem. Rev.* **2008**, *108*, 2238 – 2264.
[6] G. A. Baker, S. N. Baker, S. Pandey, F. V. Bright, *Analyst* **2005**, *130*, 800 – 808.
[7] F. Endres, M. Bukowski, R. Hempelmann, H. Natter, *Angew. Chem. Int. Ed.* **2003**, *42*, 3428 – 3430.
[8] F. Endres, S. Z. El Abedin, *Phys. Chem. Chem. Phys.* **2006**, *8*, 2101 – 2116.
[9] F. Endres, O. Höfft, N. Borisenko, L. H. Gasparotto, A. Prowald, R. Al-Salman, T. Carstens, R. Atkin, A. Bund, S. Zein El-Abedin, *Phys. Chem. Chem. Phys.* **2010**, *12*, 1724 – 1732.
[10] F. B. Sillars, S. I. Fletcher, M. Mirzaeian, P. J. Hall, *Phys. Chem. Chem. Phys.* **2012**, *14*, 6094 – 6100.
[11] P. Simon, Y. Gogotsi, *Nature Mater.* **2008**, *7*, 845 – 854.
[12] A. Lewandowski, A. Świderska-Mocek, *J. Power Sources* **2009**, *194*, 601 – 609.
[13] H. M. Srour, N. Giroud, H. Rouault, C. C. Santini, *Electrochem. Soc. Trans.* **2012**, *41*, 23 – 28.
[14] M. Grätzel, *Acc. Chem. Res.* **2009**, *42*, 1788 – 1798.
[15] H. Yuan, H. Shimotani, A. Tsukazaki, A. Ohtomo, M. Kawasaki, Y. Iwasa, *Adv. Funct. Mater.* **2009**, *19*, 1046 – 1053.
[16] F. Endres, O. Höfft, N. Borisenko, L. H. Gasparotto, A. Prowald, R. Al-Salman, T. Carstens, R. Atkins, A. Bund, S. Z. El Abedin, *Phys. Chem. Chem. Phys.* **2010**, *12*, 1724 – 1732.
[17] A. A. Kornyshev, *J. Phys. Chem. C* **2007**, *111*, 5545 – 5557.
[18] M. V. Fedorov, A. A. Kornyshev, *Electrochim. Acta* **2008**, *53*, 6835 – 6840.
[19] W. R. Fawcett, P. J. Ryan, *Phys. Chem. Chem. Phys.* **2010**, *12*, 9816 – 9821.
[20] M. Z. Bazant, B. D. Storey, A. A. Kornyshev, *Phys. Rev. Lett.* **2011**, *106*, 046102 (4 pages).
[21] M. S. Loth, B. Skinner, B. I. Shklovskii, *Phys. Rev. B* **2010**, *82*, 056102.
[22] E. I. Izgorodina, M. Forsyth, D. R. MacFarlane, *Phys. Chem. Chem. Phys.* **2009**, *11*, 2452 – 2458.
[23] E. Conway, J. O'M Bockris, I. A. Ammar, *Trans. Faraday Soc.* **1951**, *47*, 756 – 766.
[24] V. Lockett, M. Horne, R. Sedev, T. Rodopoulos, J. Ralston, *Phys. Chem. Chem. Phys.* **2010**, *12*, 12499 – 12512.
[25] M. Drüschler, B. Huber, B. Roling, *J. Phys. Chem. C* **2011**, *115*, 6802 – 6808.
[26] M. Drüschler, N. Borisenko, J. Wallauer, C. Winter, B. Huber, F. Endres, B. Roling, *Phys. Chem. Chem. Phys.* **2012**, *14*, 5090 – 5099.
[27] A. M. O'Mahony, D. S. Silvester, L. Aldous, C. Hardacre, R. G. Compton, *J. Chem. Eng. Data* **2008**, *53*, 2884 – 2891.
[28] S. Yoshimoto, R. Taguchi, R. Tsujii, H. Ueda, K. Nishiyama, *Electrochem. Commun.* **2012**, *20*, 26 – 28.
[29] C. Zhao, A. M. Bond, X. Lu, *Anal. Chem.* **2012**, *84*, 2784 – 2791.
[30] R. Atkin, N. Borisenko, M. Drüschler, S. Z. El Abedin, F. Endres, R. Hayes, B. Huber, B. Roling, *Phys. Chem. Chem. Phys.* **2011**, *13*, 6849 – 6857.
[31] M. Gnahm, T. Pajkossy, D. M. Kolb, *Electrochim. Acta* **2010**, *55*, 6212 – 6217.
[32] T. Pajkossy, *Pure Appl. Chem.* **2011**, *83*, 259 – 268.
[33] M. Gnahm, C. Müller, R. Répánszki, T. Pajkossy, D. M. Kolb, *Phys. Chem. Chem. Phys.* **2011**, *13*, 11627 – 11633.
[34] J. Vatamanu, O. Borodin, G. D. Smith, *J. Am. Chem. Soc.* **2010**, *132*, 14825 – 14833.
[35] J. Vatamanu, O. Boroding, G. D. Smith, *J. Phys. Chem. B* **2011**, *115*, 3073 – 3084.
[36] J. Vatamanu, L. Cao, O. Borodin, D. Bedrov, G. D. Smith, *J. Phys. Chem. Lett.* **2011**, *2*, 2267 – 2272.
[37] J. Vatamanu, O. Borodin, D. Bedrov, G. D. Smith, *J. Phys. Chem. C* **2012**, *116*, 7940 – 7951.
[38] M. Trulsson, J. Algotsson, J. Forsman, C. E. Woodward, *J. Phys. Chem. Lett.* **2010**, *1*, 1191 – 1195.
[39] J. Forsman, C. E. Woodward, M. Trulsson, *J. Phys. Chem. B* **2011**, *115*, 4606 – 4612.

[40] D. Henderson, J. Wu, *J. Phys. Chem. B* **2012**, *116*, 2520 – 2525.
[41] D. Jiang, D. Meng, J. Wu, *Chem. Phys. Lett.* **2011**, *504*, 153 – 158.
[42] L. B. Bhuiyan, S. Lamperski, *Mol. Phys.* **2012**, *111*, 807 – 815.
[43] N. Borisenko, S. Z. El Abedin, F. Endres, *J. Phys. Chem. B* **2006**, *110*, 6250 – 6256.
[44] K. Kirchner, T. Kirchner, V. Ivaništšev, M. V. Fedorov, *Electrochim. Acta* **2013**, in press: doi:10.1016/j.elecacta.2013.05.049.
[45] D. M. Kolb, *Angew. Chem. Int. Ed.* **2001**, *40*, 1162 – 1181.
[46] D. I. Leikis, K. V. Rybalka, E. S. Sevastyanov, A. N. Frumkin, *J. Electroanal. Chem.* **1973**, *46*, 161 – 169.
[47] G. Valincius, *J. Electroanal. Chem.* **1999**, *478*, 40 – 49.
[48] V. V. Batrakov, A. G. Makarov, *Russ. J. Electrochem.* **2003**, *39*, 1351 – 1353.
[49] O. J. Murphy, J. S. Wainright, *J. Electrochem. Soc.* **1988**, *135*, 138 – 143.
[50] A. G. Volkov, *Langmuir* **1996**, *12*, 3315 – 3319.
[51] A. Cuesta, *Surf. Sci.* **2004**, *572*, 11 – 22.
[52] U. W. Hamm, D. Kramer, R. S. Zhai, D. M. Kolb, *J. Electroanal. Chem.* **1996**, *414*, 85 – 89.
[53] G. B. Appetecchi, S. Scaccia, C. Tizzani, F. Alessandrini, S. Passerini, *J. Electrochem. Soc.* **2006**, *153*, A1685 – A1691.
[54] M. Drüschler, B. Huber, S. Passerini, B. Roling, *J. Phys. Chem. C* **2010**, *114*, 3614 – 3617.
[55] H. Sun, B. Wang, S. G. DiMagno, *Org. Lett.* **2008**, *10*, 4413 – 4416.
[56] B. Huber, B. Roling, *Electrochim. Acta* **2011**, *56*, 6569 – 6572.